Polymer 50 (2009) 279–285

Contents lists available at ScienceDirect

Polymer

journal homepage: www.elsevier.com/locate/polymer

Studies of electrospun regenerated SF/TSF nanofibers

Feng Zhang [a], Bao Q. Zuo [a,*], Huan X. Zhang [b,*], Lun Bai [a]

[a] Material Engineering Institute of Soochow University, Campus, Ganjiang Eastern Road No. 178, Suzhou, Jiangsu 215021, People's Republic of China
[b] Institute of Medical Biotechnology, Soochow University, Jiangsu Province Key Laboratory of Stem Cell, Suzhou 215007, China

ARTICLE INFO

Article history:
Received 1 April 2008
Received in revised form
30 October 2008
Accepted 31 October 2008
Available online 8 November 2008

Keywords:
SF/TSF blend
Electrospinning
Structure

ABSTRACT

The *Bombyx mori* silk fibroin/Tussah silk fibroin (SF/TSF) nanofibers with diameters between 300 and 3500 nm were prepared by electrospinning with the solvent HFIP. The average diameters of SF/TSF blend fibers increased from 404 to 1977 nm, with the increase of SF content in blend solutions, and the relationship between the average diameters of SF/TSF and SF content was proved to be linear correlation. Results from FTIR, TG-DTA and X-ray diffraction showed that the electrospun fibers were mainly β-sheet structure and, heterogeneous micro-structures. In particular, the presence of two different endothermic peaks at 300 and 360 °C in the TG-DTA curves may be ascribed to the thermal decomposition of SF and TSF. These results suggested that SF and TSF were still immiscible even dissolved in hexafluoroisopropanol (HFIP) after electrospinning and ethanol treatment. Moreover, the thermal decomposition temperature and enthalpy were improved with the blend of SF and TSF, else the SF/TSF nanofibers' moisture absorption was higher than the pure SF or TSF nanofibers. To study the cytocompatibility and cell behavior on the SF/TSF nanofibers, MSCs, VECs, and Neurons were seeded onto the nanofibers. Results indicated that the SF/TSF nanofibers promote cell attachment and spreading, suggesting that these nanofibers could be a candidate scaffold for blood vessel and nerve injury recovery.

1. Introduction

Recently, much attention has been paid to electrospinning, a very effective way to prepare nanofibers [1]. Electrospinning can be used to process many kinds of materials, like polymers, composite, ceramic materials, cellulose acetate [2,3], and so on. *Bombyx mori* silk, Sussah silk, *Samia cynthia*, recombinant hybrid silk all have been electrospun to nanofibers which are probably used in biomaterials [4–6].

B. mori silk has been used for medical suture for a long time [7]. SF (silk fibroin) is a valuable candidate materials for biomedical applications for its distinctive biomedical properties including good biocompatibility, blood compatibility, good oxygen and water permeability, biodegradability, non-cytotoxicity and minimal inflammatory reaction [8]. Tussah silk is one of the wild silks, and its chemical structure, molecular conformation and physical properties have been extensively studied [9]. In contrast to domestic silk, its amino acid composition is characterized by more Ala, Asp and Arg contents and, less Gly. Moreover, it is well known that the presence of the Arg-Gly-Asp (RGD) tripeptide sequence may act as a biological recognition signal, promoting cell adhesion and, consequently, make this protein suitable for biomedical application [10].

The aim of this study was to prepare SF/TSF blend nanofibers by electrospinning of their solution and, to characterize the microstructure properties of these nanofibers by SEM, FTIR, X-ray diffraction, and TG-DTG analyses. Furthermore, in order to evaluate the cytocompatibility and cell behavior on the SF/TSF nanofibers, MSCs, VECs, and NSCs were seeded onto the nanofibers.

2. Experimental section

2.1. Solution preparation

B. mori silk fibroin film and Tussah silk fibroin (TSF) film were made as per our previous report [11,12]. The 10% concentration spinning solutions with the SF/TSF ratios of 0/100, 20/80, 40/60, 50/50, 60/40, 80/20, 100/0 were prepared by dissolving SF film and TSF film in HFIP, and oscillating in 25 °C water bath for one week.

2.2. Electrospinning and post-treatment

The electrospinning setup used in this study consisted of a syringe and needle (0.9 mm OD × 0.5 mm ID), a rectangular (20 × 10 cm) aluminum foil collecting plate, a high voltage power supply (which can supply positive voltage from 0 to 30 kV)

* Corresponding authors.
E-mail addresses: bqzuo@suda.edu.cn (B.Q. Zuo), hzhang@suda.edu.cn (H.X. Zhang).

0032-3861/$ – see front matter Crown Copyright © 2008 Published by Elsevier Ltd. All rights reserved.
doi:10.1016/j.polymer.2008.10.053

(DW-P503-4AC, Dongwen High Voltage Power Tianjin Power Supply Plant, China), and a syringe pump (WZ-50C66 T, Medical Instrument Corporation of Zhejiang University, Zhejiang, China). The SF/TSF solutions were placed into a 10 ml syringe with a stainless needle connected the high voltage power supplier. All electrospinning experiments were performed with the same processing conditions. The distance between the flat aluminum foil and the nozzle was 12 cm. The voltage applied to the needle was 12 kV, the flow rate was 0.5 ml/h controlled by the syringe pump. As the voltage increases from 0 to 12 kV, a drop of SF/TSF solution formed at the tip of the needle, and then a jet was ejected. With the solvent evaporating, the SF/TSF blend nanofibers formed on the collection screen. The as-spun SF/TSF blend nanofibers were immersed into 75%(v/v) ethanol/water solution for 30 min to

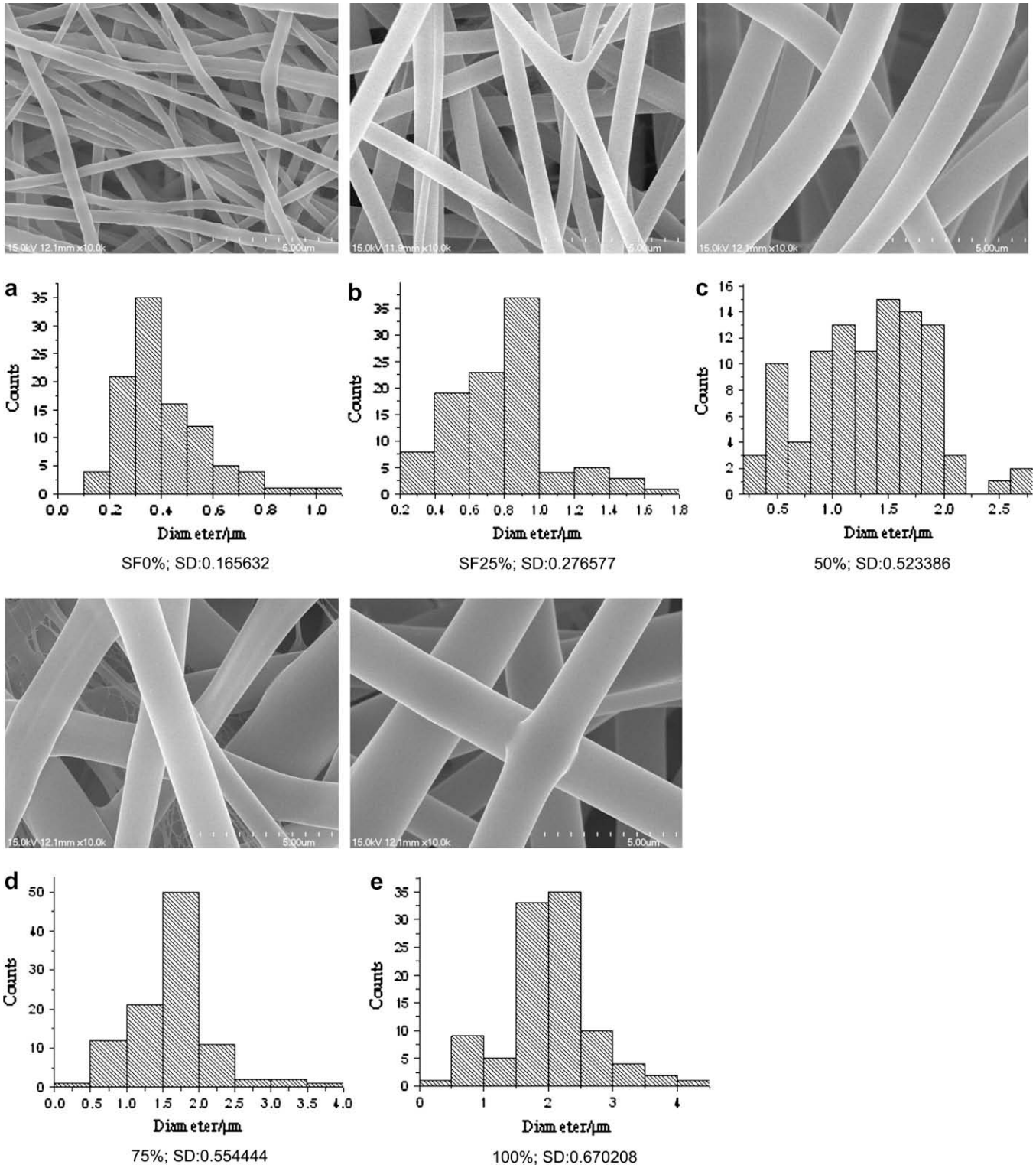

Fig. 1. SEM micrograph of the SF/TSF blend nanofibers and the distribution of the diameters.

induce the structural change, then dried at room temperature for 24 h. Samples a–g correspond to the TSF content 0%, 20%, 40%, 50%, 60%, 80%, 100%. The electrospinning experiments and post-treatment were performed at room temperature.

2.3. Characterizations

The morphology of collected SF/TSF nanofibers was observed using scanning electron microscope (SEM, Hitachi S-520, Japan) at 20 °C, 60 RH, samples were mounted on copperplate and sputter-coated with gold layer 20–30 nm thick prior to imaging, diameters of the nanofibers were acquired from SEM images randomly collected, using German Leica BME biomacroscope, for each sample, the diameter was the average of 100 measurements.

Fourier transform infrared (FTIR) spectra were obtained using a Magna spectrometer (NicoLET5700, America) in the spectral region of 400–4000 cm^{-1}, the powdered electrospun SF/TSF nanofibers were pressed into potassium bromide (KBr) pellets prior to data collection.

X-ray diffraction (X'PERT PRO MPD, PANalytical Company, Holland) was operated at 40 kV tube voltage and 40 mA tube current, CuK_α radiation was used with diffraction angle $2\theta = 2°$–45°, the scanning rate is 2°/min with powdered electrospun SF/TSF.

Thermogravimetry/differential thermal analysis (TG-DTA, PE-SII, America) conditions were nitrogen flux at 30 ml/min, heating rate at 10 °C/min and temperature range from 40 to 380 °C, and the samples' weight is about 5 mg.

2.4. Cell culture

The Electrospun SF/TSF nanofibers were collected onto the glass sheet (2 cm × 2 cm) which was placed into culture dish. To evaluate the cytocompatibility and cell behavior on SF/TSF nanofibers, three different cell sources: (a) rat bone marrow mesenchymal stem cell (MSCs), (b) vascular endothelia cells (VECs), and (c) Neuron were seeded into the 24-well plate.

Human bone marrow was obtained from normal donors, as previously described [13]. The third passage cells were digested with 0.05% trypsinisation from the culture flasks. Then cells were transferred to 24-well plate at the density of 2×10^5/ml in DMEM-LG containing 10% FBS.

Human umbilical vein endothelial cells (VECs) were obtained in our laboratory by using the method of Jaffe et al. [14]. After digestion and centrifugalization in 0.04% EDTA–0.05% trypsinisation, the third passage cells were seed onto glass sheet in 24-well plates with culture M199 medium (Gibco, USA).

Primary rat neuron cultures were prepared according to the previous reference [15]. After 12 days culture, the rat neurons were seeded onto the glass sheet which was put in the 24-well plates with a seeding density of 10^6/ml and grown in DMEM, 10% fetal calf serum (FCS) (Gibco, USA).

The glass sheets with MSCs or VECs were fixed in 10% formalin, embedded in paraffin. A standard hematoxylin and eosin (H&E) protocol was used to stain the glass sheet. Immunostaining of cultures was performed as described previously [15]. The cells of MSCs, VECs and neurons on glass sheet were examined by fluorescence microscopy (Japan, OLYMPUS CKX41).

2.5. Statistical analysis

Results are presented as mean diameters and standard deviation for $n = 100$ fibers. Statistical significance was determined in SPSS using a one-way analysis of variance (ANOVA) with a significance criterion of $P \leq 0.01$.

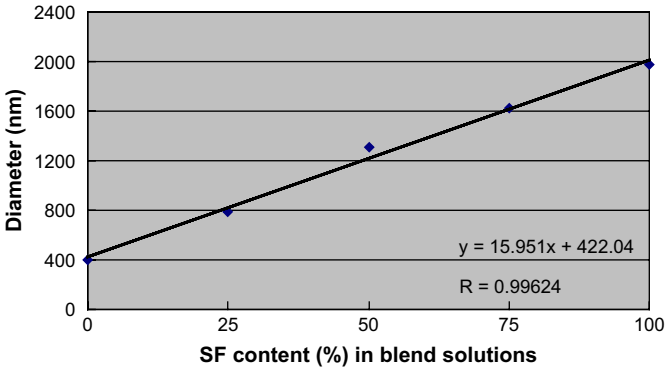

Fig. 2. Regression equation and regression straight line of the SF/TSF blend nanofibers.

3. Results and discussion

3.1. Morphological characteristics

Fig. 1 shows SEM micrographs and diameters' distribution of SF/TSF nanofibers. The ribbon-like as-spun nanofibers had a smooth surface and round cross section. Due to the incomplete solvent evaporation and jet split, fibers' adhesion and bifurcation were observed.

As shown in Fig. 1, the diameters of SF/TSF blend nanofibers were between 300 and 3500 nm, the average diameters increased from 404 to 1977 nm with the increase of SF content in blend compositions, and the diameter of five groups with different blend ratios was statistically different from each other. The reasons probably include two aspects: viscosity and conductivity. The viscosity of solutions was partially decided by SF and TSF molecular weight which were two distributions. This factor need a further research. Else the TSF contains more polar amino acid (Ap), but the SF contains more nonpolar amino acid (An), and the ratio Ap/An of SF and TSF is 0.27 and 0.33, respectively [16]. This means the TSF solution has a higher conductivity. In order to assess the effect of SF/TSF contents on the average diameters, we used experimental data to set up a linear regression equation and regression curve with unitary linear regression analysis, as shown in Fig. 2. The related coefficient (R) was calculated to test validity of equation under significance level $\alpha = 0.99$, $R = 0.99624 > 0.99116 = Ra$,

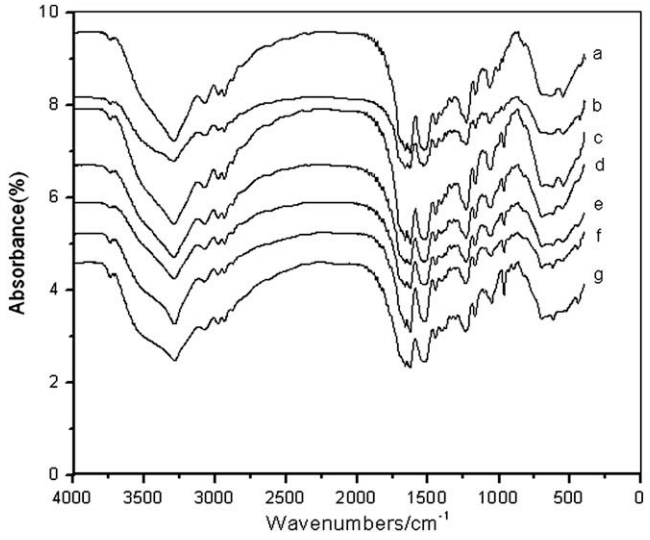

Fig. 3. FTIR spectra of the SF/TSF blend nanofibers.

Table 1
Characteristic absorption peaks of the SF/TSF blend nanofibers.

	Amide I		Amide II		Amide III	Amide IV		Amide V		
a	1661.7	1626.6	1514.7	1531.7	1232.1			696	645.3	
b	1661.5	1627.0	1521.8	1531.0	1232.2	969.8		700.1	648.7	627.3
c	1661.7	1626.0	1518.2	1530.9	1231.5	966.5		700.1	650.1	621.9
d	1661.6	1627.6	1516.4	1531.4	1233.4	966.2		696	660.0	626
e	1661.6	1627.2	1516.4	1531.3	1232.4	966.0		700.5		622.3
f	1661.4	1626.8	1518.3	1531.2	1235.8	969.8		698.6		622.2
g	1661.6	1627.4	1518.2	1531.3	1237.9	965.4	895.2	700		620.4

demonstrating that the regression equation was valuable with 99.9% degree of confidence.

3.2. Structural analysis

3.2.1. FTIR

IR is a powerful and common tool for the protein conformation analysis, and therefore is widely used in the study of silk protein [17]. The IR spectra of seven SF/TSF blend nanofibers showed similar characterized absorption peaks (Fig. 3). Table 1 shows amides corresponding to characteristic absorption peaks.

As shown in Fig. 3 and Table 1, the β-sheet and α-helix structure co-existed in the SF/TSF blend nanofibers. The spectrum of SF nanofibers was characterized by the absorption bands at 1626, 1514, 696 cm^{-1}, attributed to the β-sheet and at 1661, 1531, 1232, 645 cm^{-1} due to the α-helix or random coil conformation. The corresponding absorption bands for the TSF nanofibers were at 1627, 1518, 1237, 965, 700 cm^{-1}, attributed to the β-sheet and at 1661, 1531, 895, 620 cm^{-1} due to the α-helix.

The IR spectra of the blend nanofibers (b–f) were quite similar to each other, and showed absorption bands characteristic of both SF and TSF pure components overlapping in the corresponding absorption region examined. Nevertheless, various small modifications were observed in the IR spectra with proportion of SF/TSF changing. The TSF absorption peak at 895 (amide IV) attributed to α-helix will disappeared, and the absorption peak at 620.4 cm^{-1} (amide V) due to random coil will transfer from low wavenumbers to high wavenumbers with the increase of SF in the blends. At the same time, the SF absorption peak at 645 cm^{-1} (amide V) attributed to random coil will transfer from low wavenumbers to high wavenumbers too. These modifications seem to indicate an increase of β-sheet content. The SF/TSF nanofibers post-treated with 75% ethanol mainly contained β-sheet conformation, also α-helix and random coil conformation existed. This probably indicated that the blend of SF and TSF facilitated the conformational transition of the electrospun SF/TSF nanofibers from random coil/silk I conformation to silk II conformation. No additional bands were detected, suggesting that the molecular interactions between SF and TSF are very weak or even absent in the blend nanofibers [18].

Table 2
Diffraction peaks and spacing corresponding to silk I and silk II of TSF [16,18,20].

Silk I		Silk II	
d (Å)	2*θ* (°)	*d* (Å)	2*θ* (°)
7.69	11.50	5.40	16.40
7.40	11.95	5.30	16.71
7.25	12.20	4.43	20.00
4.03	22.00	4.26	20.34
3.95	22.50	4.33	20.50
3.86	23.00	3.73	23.80
3.78	23.50	3.63	24.49
3.70	24.02	3.78	25.50
		2.89	30.90
		2.59	34.59
		2.20	40.97
		2.05	44.12

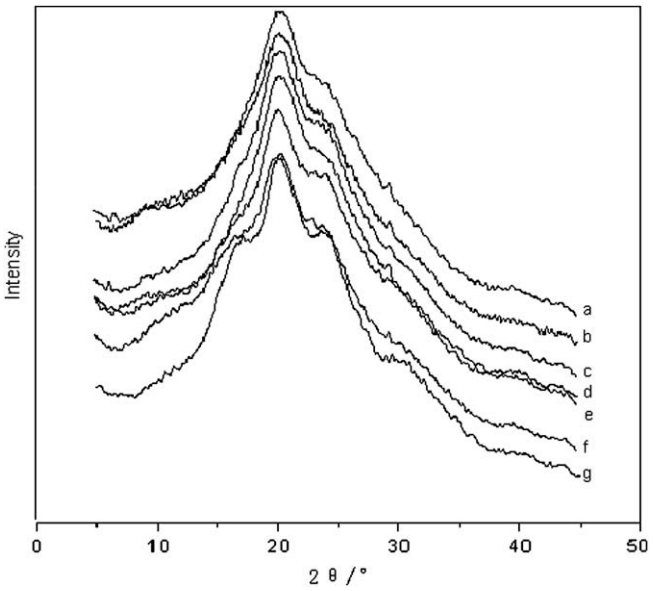

Fig. 4. X-ray diffraction pattern of the SF/TSF blend nanofibers.

3.2.2. X-ray diffraction curves

X-ray diffraction was carried out to study the crystalline structure of the SF/TSF nanofibers. Table 2 shows diffraction peaks corresponding to silk I and silk II of TSF. The diffraction peaks due to silk I and silk II of SF had been summarized by Wu et al. [19].

Fig. 4 shows the diffraction pattern of the SF/TSF blend nanofibers. The pure SF nanofibers [21] exhibited three diffraction peaks at 20.6, 24.3, 9.8° corresponding to the spacing of 4.31, 3.66, 8.96 Å, attributed to silk II, and 29.4° corresponding to the spacing of 3.03 Å due to silk I. The pure TSF nanofibers showed diffraction peaks at 17.3, 20.4, 23.8° corresponding to the spacing of 5.12, 4.35, 3.73 Å, attributed to silk II. From the IR analysis, we know that the molecular interaction between SF and TSF is very weak or absent. Consistent with these results, the diffraction pattern of the blend nanofibers (b–f) exhibited diffraction peaks' characteristic of SF and TSF simply overlapping in Fig. 4. However, the diffraction peak at

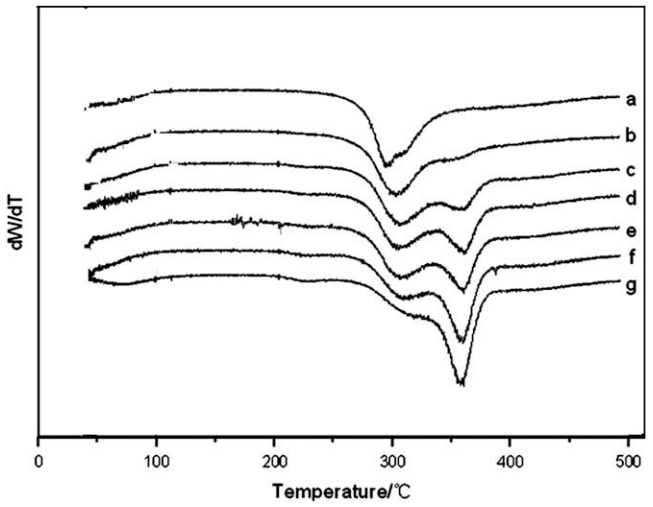

Fig. 5. DTG curve of the SF/TSF blend nanofibers.

17.3° characteristic of TSF disappeared when the SF content is up to 60%, demonstrating that the blending of SF/TSF has affected the crystal structure of TSF. The low dispersed TSF concentration may reduce the probability of TSF chains' aggregation and β-formation. As shown in DTA curve, the TSF decomposition peak is small and wide when the SF content is 60%, and the decomposition peak disappears when the SF content is 80%. In FTIR spectra, the absorption peak at 965 cm^{-1} attributed to the β-sheet was hard to be observed when the SF content is 80%. These results suggested that the β-sheet formation of TSF was prevented when the TSF content is low to 40%.

3.3. Thermal and moisture absorption properties

3.3.1. DTG curve

As shown in Fig. 5, pure SF and TSF nanofibers both had a single decomposition peak at 294 and 357 °C, but the blend nanofibers (c–f) all had two decomposition peaks corresponding to pure SF and TSF. It illustrated that the two silk fibroins didn't form co-crystal structure; the SF crystal region and TSF crystal region co-existed in blend nanofibers. SF and TSF were still immiscible even after HFIP dissolve, electrospinning and ethanol treatment, as reported previously [17].

The thermal decomposition process of blend nanofibers was composed of two stages: SF and TSF thermal decomposition, as shown in Table 3. They have two different DPTs (decomposition peak temperature) near 300 and 360 °C respectively which were decided by their different crystal structure. The SF and TSF are mainly $-(GX)_n-$ (where G is glycine and X is alanine or serine) and –(ala)– repeats in the polypeptide sequences of the crystalline regions, respectively [16,22]. So the TSF molecular chains would form a more compact crystalline structure than SF (Fig. 5) and had different diffraction peaks with SF (Fig. 4). The TSF decomposition temperatures, including DBT (decomposition beginning temperature), DPT, and DET (decomposition ending temperature) were obviously higher than SF. On the SF decomposition stage, the blend nanofibers' DPT was higher than pure SF nanofibers' because the increase of more thermal stability TSF made the thermic transfer harder and thereby improved the blend nanofibers' thermal stability. On the TSF decomposition stage, the addition of less thermal stability SF also increases the blend nanofibers' DPT. The explanation was that the remains of SF decomposition interfered the thermic transfer, the more SF content in the blend nanofibers, the more obvious effect, and the higher DPT. Furthermore, the little increase in decomposition peak with increasing the other component was because the presence of interchain crosslinks with the molecules has little effect on decomposition process [23].

Table 3
DTG data of the SF/TSF blend nanofibers.

Sample	TG primary stage					TG second stage		
	DBT/T_i (°C)	RBD ΔW_i/%	DPT T_{pd}/°C	DET T_f/°C	RDE ΔW_i/%	DPT T_{pd}/°C	DET T_f/°C	RE ΔW_f/%
a	277.2	93.2	294.2	334.7	66.3			38.3
b	277.9	86.4	301.4	327.6	64.2		375.8	40.7
c	284.6	86.1	305.1	335.2	63.0	360.7	378.7	34.1
d	283.5	89.7	304.0	336.1	64.6	360.7	377.7	32.0
e	280.1	86.7	305.3	338.0	63.2	359.8	376.7	31.4
f	286.4	85.8	308.8	338.0	65.9	359.3	375.8	29.3
g				339.4	71.1	357.4	375.8	31.4

Decomposition beginning temperature (DBT); remains at the beginning decomposition (RBD); decomposition peak temperature (DPT); decomposition ending temperature (DET); remains at the decomposition ending (RDE); remains in the end (RE).

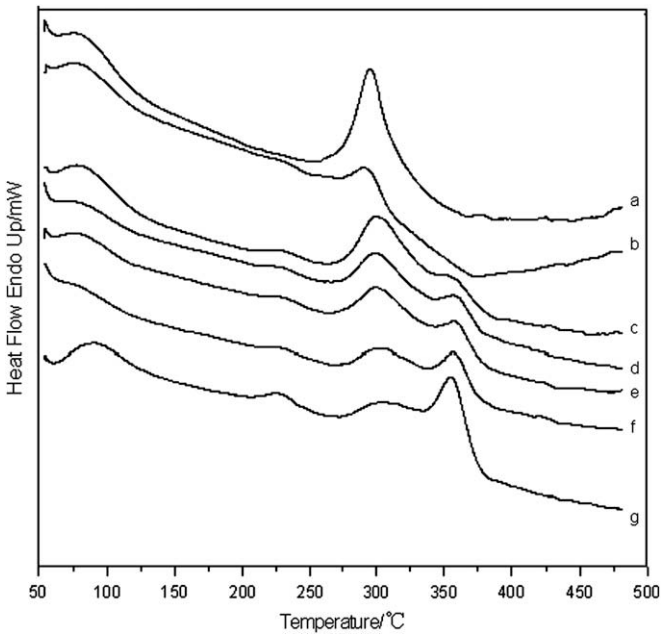

Fig. 6. DTA curve of the SF/TSF blend nanofibers.

Table 4
Descompostion endotherm data of the SF/TSF blend nanofibers.

Sample	Heat quantity absorption (J)	Heat quantity absorption per gram (J/g)
a	790.469	150.8036
b	205.592	103.9077
c	786.234	167.2578
d	608.626	168.0299
e	301.46	168.4357
f	502.563	162.4031
g	351.044	75.2389

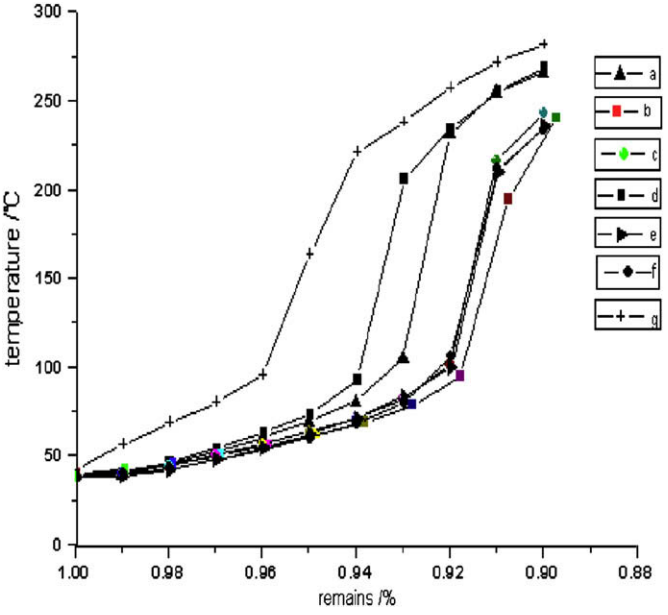

Fig. 7. Weight loss–temperature curve of the SF/TSF blend nanofibers.

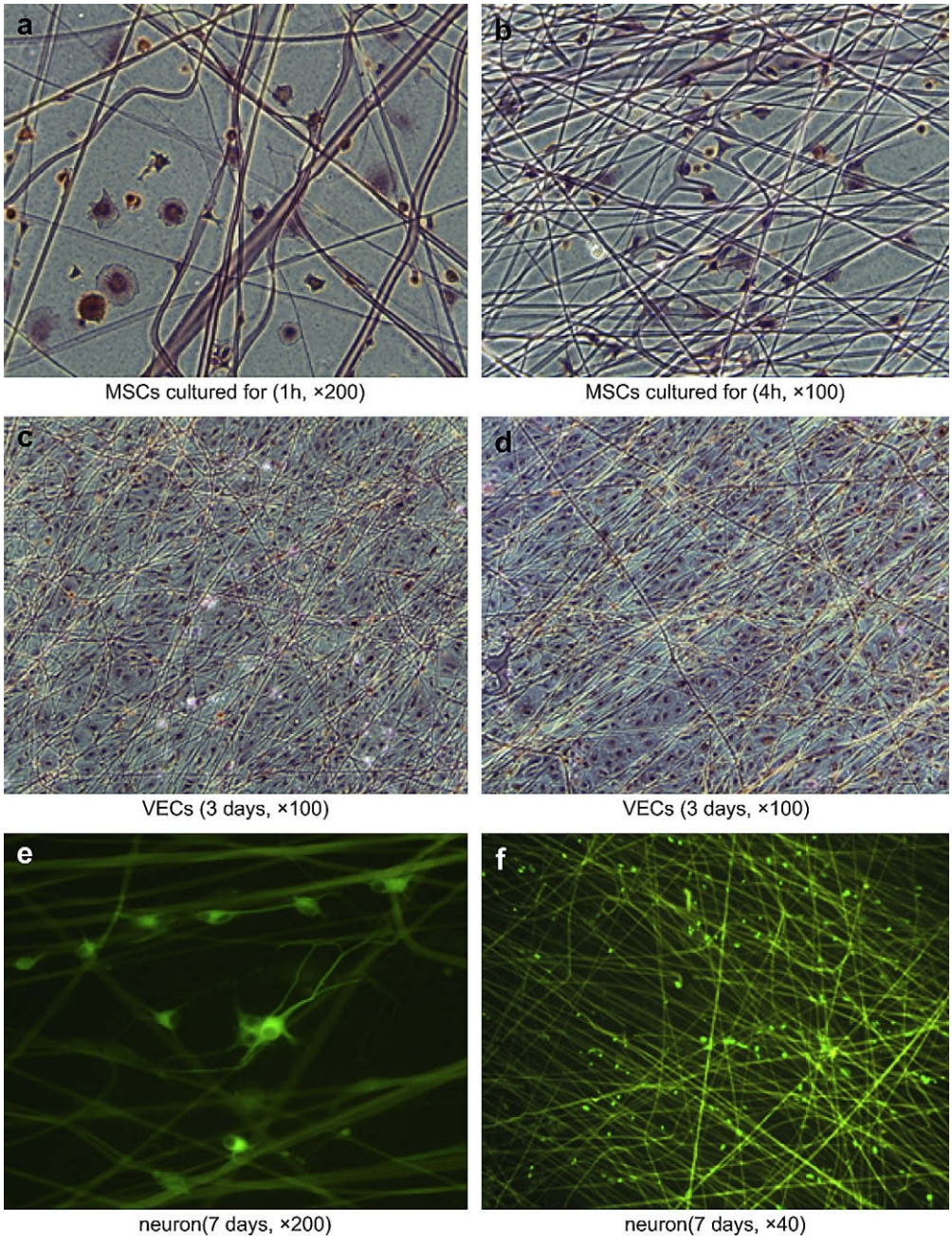

Fig. 8. Morphology of cells cultured on the electrospun SF/TSF nanofibers.

3.3.2. DTA analysis

As shown in Fig. 6, the endothermic and exothermic peaks occurred in the range of 200–400 °C and the first small endotherm near 100 °C was due to the evaporation of water. There were two prominent endothermic peaks near 300 °C and 360 °C corresponding to the thermal decomposition of SF (oriented β-sheet structure) and TSF (unoriented β-sheet structure) [19,20]. The thermal decomposition peak of SF or TSF shifted to higher temperature with the increase of TSF or SF content. It demonstrated that the SF/TSF blend nanofibers gained a higher thermal decomposition temperature. The thermal decomposition peak of SF contained mainly random coil and silk I conformation was 266–269 °C [21]. The regenerated TSF exhibited an endo–exo transition at around 230 °C [18,20,24–26]. There was a small endo–exo peaks appeared near 220 °C which has been associated with structural changes (α-helix or random coil to β-sheet conformation), suggesting that the TSF contained mainly β-sheet conformation after ethanol post-treatment. The diffraction peaks of TSF in the XRD pattern all were attributed to silk II, and the decomposition peak of TSF in DTG is 357 °C corresponding to β-sheet structure. These results are consistent with the DTA result.

There was a direct ratio relationship between DTA peak area and denaturation enthalpy [27] which reflecting the corresponding crystallinity [23]. As shown in Table 4, the SF/TSF blend nanofibers' peak area exceeded the pure nanofibers' (except sample b), indicating that the thermal decomposition of blend nanofibers needed more enthalpy change.

Fig. 7 is from the DTA data. The aim was to investigate the relationship between weight loss and temperature under small weight loss and low temperature, and to study moisture absorption

performance of the blend nanofibers. As shown in Fig. 8, under the same temperature the blend nanofibers lost more weight, and under the same weight loss, the blend nanofibers needed lower temperature. It was reported that the weight loss of silk fibroin was mainly water evaporation below 200 °C [19,28]. So, we believed that the blend nanofibers had higher moisture absorption performance than pure nanofibers.

3.4. Cell behavior

Scaffold materials for tissue engineering are required to support cell adhesion, growth and physiological and physical function and to maintain normal states of cell differentiation [5]. Therefore, a primary study on the cytocompatibility of SF/TSF nanofibers is especially important in relation to its potential application in tissue engineering.

To assess the initial cell attachment and spreading, MSCs, VECs and Neurons were seeded onto the SF/TSF nanofibers. As shown in Fig. 8a and b stained with hematoxylin and eosin (H&E), some MSCs didn't adhere to nanofibers after cultured in 1 h, but after 4 h, almost all cells were attached to the nanofibers, demonstrating that the MSCs moved to and adhered to the nanofibers during the culture time. The growth patterns of VECs are closely related to the arrangement of nanofibers: if the nanofiber arrangement in the mats was random, the cells' alignment was random; if the nanofiber was in parallel arrangement to some extent, the cells were arranged along the nanofibers, as shown in Fig. 8c and d stained with H&E. The Neurons were also attached to the nanofibers, and we found that the cells' dendrites not only grasp one single nanofiber, but several nanofibers nearby, as shown in Fig. 8e and f. These results proved the compatibility between cells and nanofibers. Further study is needed to identify the appropriate blend ratio and electrospinning parameters to prepare SF/TSF nanofibers scaffolding used for tissue engineering.

4. Conclusions

In this study, the SF and TSF dissolved in HFIP were electrospun into nanofibers with the blend ratios of 100/0, 80/20, 60/40, 50/50, 40/60, 20/80, 0/100. A linear correlation was found between the average diameters and SF or TSF content. The estimated structure and physical properties of electrospun SF/TSF blend nanofibers suggest that the two fibrous proteins have low degree of compatibility after electrospinning. After 75% ethanol treatment, random coil, α-helix and β-sheet co-exist in the electrospun nanofiber mats. Compared with the electrospun pure SF and TSF mats, the SF/TSF blend mats exhibited higher thermal deposition property and excellent moisture absorption performance. In the cell culture assessment, the SF/TSF blend nanofibers were found to support cell adhesion and spreading of MSCs, VECs and Neurons. These results may indicate that SF/TSF blend nanofibers are functionally active in terms of cell attachment and spreading, and a promising candidate scaffold materials for tissue engineering.

Acknowledgement

The present work is supported financially by the Natural Science Foundation of Jiangsu (No. BK2007054) and Sponsored by National Base Research Program of China (973 program) (2005CB623906).

References

[1] Huang ZM, Zhang YZ, Kotaki M, Ramakrishna S. Compos Sci Technol 2003; 63:2223.
[2] Chronakis IS. J Mater Process Technol 2005;167:283.
[3] Sunwantong O, Opanasopit P, Ruktanonchai U, Supaphol P. Polymer 2007;48:7546.
[4] Ohgo K, Zhao CH, Kobayashi M, Asakura T. Polymer 2003;44:841.
[5] Park KE, Jung SY, Lee SJ, Min BW, Park WH. Int J Biol Macromol 2006;38:165.
[6] Chen C, Cao CB, Ma XL, Tang Y, Zhu HS. Polymer 2006;47:6322.
[7] Moy RL, Lee A, Zalka A. Am Fam Physician 1991;44:2123.
[8] Yao JR, Chen X, Shao ZZ, Zhou P, Chen G, Mei N, et al. J Fudan Univ (Nat Sci) 2003;42:828.
[9] Lucas F, Shaw JTB, Smith SG. J Mol Biol 1960;2:339.
[10] Pierschbacher MD, Ruoslahti E. Nature 1984;309:30.
[11] Zuo BQ, Liu LG, Wu ZY. J Appl Polym Sci 2007;106:53.
[12] Zuo BQ, Zhang F, Sun CG, Bai L. Polym Mater Sci Eng 2007;23:207.
[13] Luan XY, Duan QY, Duan X, Wang Y, Li MZ, Lu SZ, et al. Chin J Biomed Eng 2007;26:276.
[14] Jaffe EA, Nachman RL, Becker CG, Minick CR. J Clin Investig 1973;52:2745.
[15] Zhang HX, Vutskits L, Pepper MS, Kiss JZ. J Cell Biol 2003;163:1375.
[16] Freddi G, Gotoh Y, Tsutsui T, Tsukada M. J Appl Polym Sci 1994;53:775.
[17] Zhou W, Chen X, Shao ZZ. Prog Chem 2006;18:1514.
[18] Tsukada M, Freddi G, Kasai N. J Polym Sci Part B Polym Phys 1994;32:1175.
[19] Wu WY, Jin ZM, Xu LQ. Acta Sericol Sin 1993;19:105.
[20] Kweon HY, Woo SO, Park YH. J Appl Polym Sci 2001;81:1467.
[21] Zhu JX, Zhang YP, Shao HL, Hu XC. Polymer 2008;49:2880.
[22] Inoue S, Magoshi J, Tanaka T, Magoshi Y, Becker M. J Polym Sci Part B Polym Phys 2000;38:1436.
[23] Zhang YZ, Venugopal J, Huang ZM, Lim CT, Ramakrishna S. Polymer 2006; 47:2911.
[24] Tao W, Li MZ, Lu SZ, Liu JJ, Wu ZY. J Donghua Univ (Nat Sci Ed) 2005;31:23.
[25] Kweon HY, Park YH. J Appl Polym Sci 1999;73:2887.
[26] Kweon HY, Um IC, Park YH. Polymer 2000;41:7361.
[27] Wang SH, Yang HZ. The application of DTA analysis. Beijing: Beijing Normal University Press; 1981. p. 42.
[28] Feng YF, Feng XF, Xu H. J Zhejiang Silk Eng College 1986;3:1.